Influence of the lattice parameter of the AlN buffer layer on the stress state of GaN film grown on (111) Si

Zhen-Zhuo Zhang(张臻琢)[1,2], Jing Yang(杨静)[1,†], De-Gang Zhao(赵德刚)[1,3,‡], Feng Liang(梁锋)[1], Ping Chen(陈平)[1], and Zong-Shun Liu(刘宗顺)[1]

[1] *State Key Laboratory of Integrated Optoelectronics, Institute of Semiconductor, Chinese Academy of Sciences, Beijing* 100083, *China*
[2] *College of Materials Science and Opto-Electronic Technology, University of Chinese Academy of Sciences, Beijing* 100049, *China*
[3] *Center of Materials Science and Optoelectronics Engineering, University of Chinese Academy of Sciences, Beijing* 100049, *China*

(Received 15 March 2022; revised manuscript received 7 April 2022; accepted manuscript online 28 April 2022)

GaN films grown on (111) Si substrate with different lattice parameters of the AlN buffer layer by metal–organic chemical vapor deposition are studied. The stress states obtained by different test methods are compared and it is found that the lattice parameter of the AlN buffer layer may have a significant effect on the stress state in the initial stage of subsequent GaN film growth. A larger compressive stress is beneficial to improved surface morphology and crystal quality of GaN film. The results of further orthogonal experiments show that an important factor affecting the lattice parameter is the growth rate of the AlN buffer layer. This work may be helpful for realizing simple GaN-on-Si structures and thus reducing the costs of growth processes.

Keywords: GaN, Si substrate, AlN buffer layer, stress control

PACS: 81.05.Ea, 81.15.Gh **DOI:** 10.1088/1674-1056/ac6b2b

1. Introduction

As a wide band gap semiconductor, GaN is attracting increasing attention in microelectronics and optoelectronics devices, such as high electron mobility transistors (HEMT),[1] light emitting diodes (LED),[2] and laser diodes (LD).[3] Compared to sapphire, SiC and GaN, using Si as the substrate is expected to reduce costs and achieve integration. Unfortunately, the reaction between Ga and Si, namely, the melt-back etching effect, and the large mismatch in lattice constants (17%) and thermal expansion coefficients (56%) between Si and GaN severely restrict the development of GaN-on-Si growth technology.[4] Choosing AlN instead of GaN as the material of the buffer layer is an effective way to isolate Ga atoms from Si and thus avoid melt-back etching.[5] To solve the mismatch in the coefficient of thermal expansion (CTE) and reduce the high density of threading dislocations (TDD) causing by the large lattice mismatch, several methods were used to enhance compressive stress to compensate the tensile stress generated during the cooling process and also to reduce the threading dislocations during the growth process, such as using a multiple AlGaN intermediate layer,[6] low temperature AlN (LT-AlN) insert layer,[7] AlGaN/GaN superlattice buffer layer[8] and so on. Nevertheless, these techniques have to introduce additional layers into the system, and the complicated techniques would reduce device reliability and would not be conducive to cost reduction,[9] which is one of the original purposes of GaN-on-Si growth technology.

A GaN/AlN heterostructure interface can introduce a theoretically large enough compressive stress in both the growth process and cooling process due to the smaller lattice parameter and smaller thermal expansion coefficient of AlN compared to GaN.[10] However, it is known that the growth mode of the AlN buffer layer on Si is normally the Vollmer–Weber mode and its initial stage is nucleation and island coalescence.[11] A high TDD will be unavoidably formed in the AlN buffer layer during the coalescence of island boundaries.[12] Due to the high TDD in the AlN buffer layer, the compressive stress relaxes and transforms to tensile stress due to the low quality AlN buffer layer[13,14] and thus an ideal result cannot be achieved.

Nowadays, with deepening understanding of AlN crystal growth, a higher quality AlN buffer layer can be achieved.[15,16] Therefore, the hope of using a simple buffer layer structure to realize crack-free GaN-on-Si has been rekindled again in recent years.[16–24] In this field, some teams focus on optimizing TMA[20,21] or ammonia[22,23] preflow conditions or AlN buffer layer design by modifying the temperature[12,16,25] to further improve the quality of the AlN buffer layer, and thus increase the compressive stress applied to GaN and achieve thicker crack-free GaN-on-Si with a low density of threading dislocations. However, due to the huge lattice mismatch between AlN and Si (19%), the thickness of AlN is limited to several hundred nanometers,[16] which also limits the further improvement of the quality of the AlN buffer layer.[26] Thus, improving the quality of the AlN buffer layer

†Corresponding author. E-mail: yangjing333@semi.ac.cn
‡Corresponding author. E-mail: dgzhao@red.semi.ac.cn

© 2023 Chinese Physical Society and IOP Publishing Ltd

is not easy, and additional measures need to be found.

In this work, it is found that the in-plane stress at the initial stage of GaN growth is sensitive to the lattice parameter of the AlN buffer layer. The results of further orthogonal experiments show that the most important factor affecting the lattice parameter of the AlN buffer layer is its growth rate. By optimizing the lattice parameter of the AlN buffer layer, a 0.8 μm thick GaN film without cracks (except the edge zone) and with full widths at half maximum (FWHM) for (002) and (102) x-ray diffraction (XRD) rocking curves of 717 arcsec and 838 arcsec, respectively, are achieved.

2. Experiment

AlN and GaN were all grown on a 2-inch (111) Si substrate by an Aixtron 6×2 inch close-coupled showerhead reactor metal–organic chemical vapor deposition (MOCVD) system. The (111) Si substrate wafer used in the MOCVD growth was prepared by the floating-zone technique and was epi-ready. The resistivity of the substrate was higher than 1000 Ω·cm. Due to the vacuum package and the N_2 atmosphere in the glove box, no additional cleaning procedure was needed before the Si wafer was moved into the reaction chamber. Trimethygallium (TMG), trimethylaluminum (TMA), and ammonia (NH_3) were used as the Ga, Al and N sources, and H_2 and N_2 were used as carrier gases. The Si substrate was baked at ∼ 1050 °C in a H_2 atmosphere for 5 min to remove the native surface oxidation layer. Then, TMA was introduced in the reactor to prevent the formation of amorphous Si_xN_y due to the possible reaction between the Si substrate and residual ammonia in the reactor. Subsequently, ammonia was introduced into the reactor and an AlN buffer layer with a thickness of 200 nm was grown. The main growth parameter variables of these three samples are listed in Table 1. Other parameters except those listed in Table 1, such as the thickness of the AlN buffer layer, V/III mole ratio and so on, were kept constant (the growth rate was controlled by modifying the flow rates of MO sources and ammonia). After the growth of AlN, 0.8 μm GaN films were grown at 1050 °C on the AlN buffer layer under the same condition. The reactor pressures of AlN and GaN growth were 100 mbar and 260 mbar, respectively.

Table 1. Main growth conditions of the AlN buffer layers for samples A, B, and C.

	Sample A	Sample B	Sample C
TMA preflow time (s)	20	30	60
Growth rate (nm/s)	0.056	0.083	0.067
Growth temperature (°C)	1025	1075	1050

The *in-situ* curvature of the samples was monitored during MOCVD growth by Lay-tec EpiCurve®TT software. The Raman spectra of the three samples were measured at room temperature by 532 nm laser excitation. The FWHM of the rocking curves were measured by triple-axis high resolution x-ray diffraction (HRXRD). HRXRD was performed employing a Cu $K_{\alpha 1}$ line of wavelength $\lambda = 0.15406$ nm. The surface morphology was examined by a Normaski microscope and atomic force microscope (AFM).

3. Results and discussion

The *in-situ* curvature curves measured during the GaN layer growth of samples A, B and C are plotted in Fig. 1. The mean stress during the epitaxy process at growth temperature can be deduced from the slope of the curve according to Stoney's formula[14]

$$\sigma_{\mathrm{m}} = \frac{E_{\mathrm{s}} h_{\mathrm{s}}^2}{6 h_{\mathrm{f}} (1 - \nu_{\mathrm{s}})} \kappa, \tag{1}$$

where σ_{m} is the mean stress applied to the film, E_{s} is the Young modulus of the substrate and equals 1.85×10^{11} N/m^2 for Si,[27] ν_{s} is the Poisson ratio of the substrate and equals 0.26,[27] h_{s} is the thickness of the Si substrate and equals 430 μm, h_{f} is the thickness of the grown film, and κ is the measured curvature.

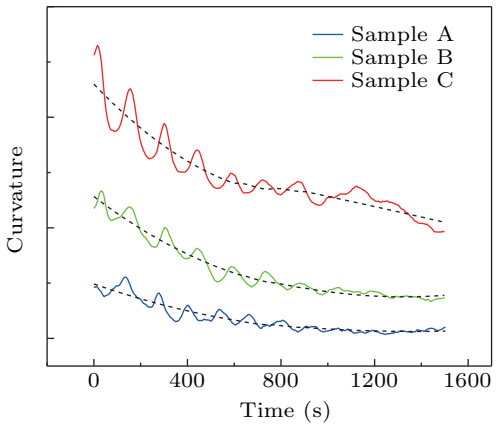


Fig. 1. *In-situ* curvature value versus time for the growth of three GaN films on different AlN buffer layers. The solid curves are the ones recorded during the measurement where the additional undulations are a normal phenomenon caused by optical interference. The dotted curves are plotted after smoothing treatment of the original data. These curves show only their patterns but not the calibrated value of curvature.

After a calibration treatment and differentiating, the initial stress of the interface between AlN and GaN is calculated as −0.432 GPa, −0.955 GPa, and −1.359 GPa, where the negative sign represents that the stress is compressive. The fact that the absolute value of the slope gradually decreases indicates the relaxation of compressive stress. It can be seen that the compressive stresses in the three samples do not completely transform to tensile stress during the growth of 0.8 μm thick GaN film, indicating the high quality of the AlN buffer layers.[13,14]

Figure 2 shows the HRXRD ω–2θ scan diffraction patterns of the samples. The typical results of triple-axis ω–2θ scans from Si(111), GaN(002), AlN(002), GaN(004), and

AlN(004) reflection are marked in Fig. 2(a). In order to confirm the lattice constant from the ω–2θ scans, scanning with high precision was done near the peak positions of GaN(004) and AlN(004). The lattice parameters can be calculated by Bragg's law[28]

$$2d_{\perp}\sin\theta = n\lambda, \tag{2}$$

where $d_{\perp}$ is the c-plane lattice parameter actually measured, n is the diffraction order, which equals 4 in this experiment, and λ is the wavelength of the x-rays, which equals 0.15406 nm. The step length of the scanning is 0.0001° and the error can be obtained by differentiating Bragg's law to give[28]

$$\frac{\Delta d_{hkl}}{d_{hkl}} \approx \cot\theta_{hkl}\cdot\Delta\theta, \tag{3}$$

where $\Delta\theta$ is the step length of the scanning and the error in the c-plane lattice constant is calculated as $\pm$0.00006 nm. It can be seen in Fig. 2(b) that the positions of the GaN peaks are nearly the same, which indicates that the lattice constants of the GaN film are very close. However, the positions of the AlN peaks are quite different in Fig. 2(c), which indicates that the c-plane lattice parameters of the AlN buffer layer in these samples are modified. Using Eq. (2), the c-plane lattice parameters of AlN of sample A to sample C are calculated as 0.49655 nm, 0.49690 nm, and 0.49727 nm, respectively. Due to the thin thickness and high TDD of the AlN buffer layer, the intensity of high-angle HRXRD asymmetric diffraction is too low. Hence, the in-plane lattice parameter of the AlN buffer layer cannot be accurately obtained by HRXRD for these samples. However, since there is an inverse correlation between the c-plane and in-plane lattice parameter, it can be inferred that the in-plane lattice parameter decreased sequentially from sample A to sample C.

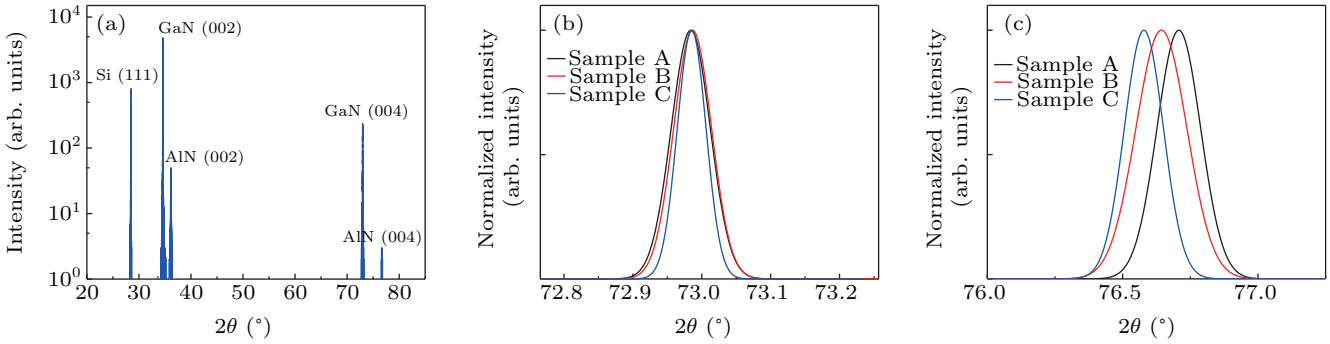


Fig. 2. (a) Diffraction peaks of sample C are obtained from rapid ω–2θ scans of triple-axis XRD. Precise ω–2θ scans of (b) the peak of GaN(004) and (c) the peak of AlN(004). In order to better compare the three sample displacements in 2θ, the peak intensity is normalized in (b) and (c).

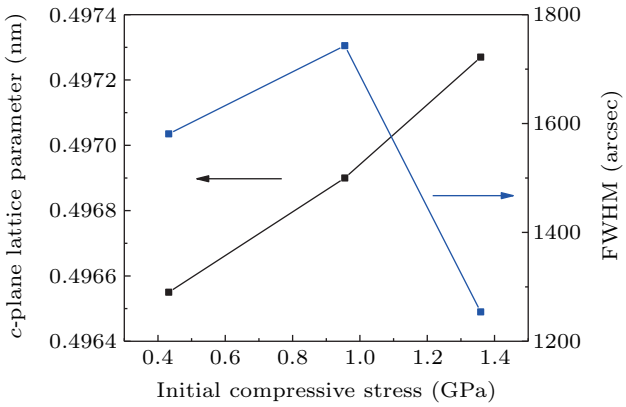


Fig. 3. Lattice parameter and FWHM value of XRD (002) rocking curve of the AlN buffer layer dependent on the initial compressive stress.

As was suggested, improving the crystal quality of the AlN buffer layer could increase the compressive stress and reduce the stress relaxation in the subsequently grown GaN film.[9] However, sample B, which has a relatively lower crystal quality than sample A, has a stronger compressive stress than sample A. Therefore, it can be inferred that other factors may also influence the stress states. If we suppose that the GaN was coherently grown on the AlN buffer layer at the initial growth stage of GaN, the stress applied on GaN caused by lattice mismatch can be deduced by Hooke's law

$$\sigma_{\mathrm{GaN}} = \frac{a_{\mathrm{AlN}} - a_{\mathrm{GaN}}}{a_{\mathrm{GaN}}}\cdot E_{\mathrm{GaN}}, \tag{4}$$

where σ_{GaN} is the stress applied to GaN film, and E_{GaN} is the Young modulus of GaN and equals 466 GPa.[30] If we assume that in the three samples their stress difference is caused by the lattice mismatch, we can roughly estimate the in-plane lattice difference of the AlN buffer layer since the lattice constants of GaN are basically the same as we mentioned before. According to *in-situ* monitoring, the stress difference between sample A and sample C is 0.927 GPa and the in-plane lattice difference of the AlN buffer layer should be 0.00063 nm. For an ideal crystal of AlN film under biaxial stress, the difference in the in-plane lattice parameter mentioned above will change the c-plane lattice parameter by 0.00078 nm, which is comparable to the difference obtained by HRXRD (0.00072 nm). Hence, we speculate that the compressive stress applied to the GaN film was probably changed by the difference in the lattice parameter of AlN buffer layer.

Raman spectra were also measured at room temperature by 532 nm laser beam excitation to show the final stress state of GaN films after the cooling process as shown in Fig. 4.

Since the E_2 (high) phonon peak is non-polar and sensitive to the biaxial stress, it is usually used to check the stress state in the sample[32] according to the formula shown below:[33]

$$\Delta\omega = K \cdot \sigma, \tag{5}$$

where $\Delta\omega$ is the shift of the E_2 (high) peak compared to the value ω in the intrinsic condition, where ω is 567.6 cm^{-1}[34] for GaN and K is 4.3 $cm^{-1}\cdot GPa^{-1}$ which represents the stress coefficient[35] for GaN. The residual stresses in the GaN films of samples A, B, and C at room temperature in the GaN film were calculated as 0.68 GPa, 0.57 GPa, and 0.49 GPa respectively, and they were all tensile stress. The tensile stresses should be mainly generated during the cooling process and were not fully compensated by the compressive stress induced at the GaN/AlN heterostructure. The decreasing trend of residual tensile stress from sample A to sample C shows the increasing compressive stress applied to GaN during the growth. Herein from the result of Raman spectra the difference of stress between sample A and sample C is 0.19 GPa, which is far less than those estimated from the *in-situ* curvature monitor. This shows that there might be additional ways to relax the tensile stress from CTE mismatch during or after the cooling process.

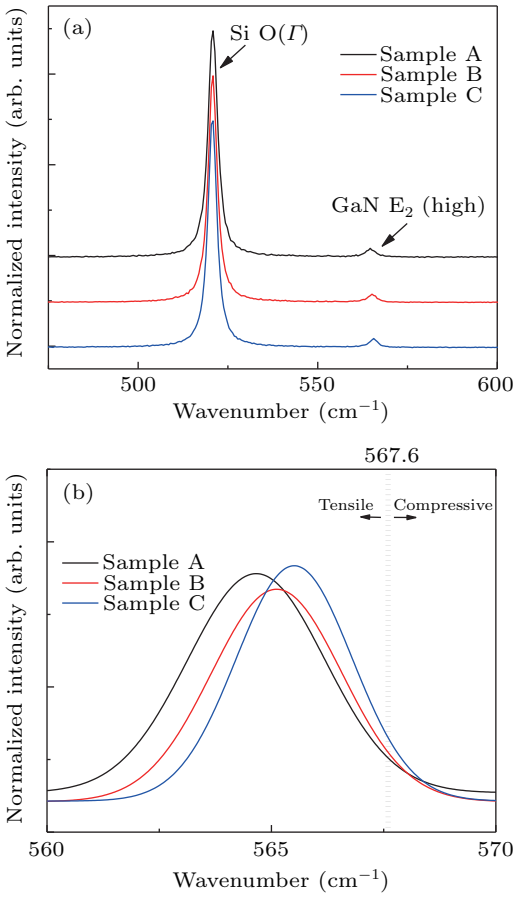


Fig. 4. (a) Raman spectra of three GaN film samples which are grown with different AlN buffer layers on Si. (b) Details of the Raman shift of the GaN E_2 (high) peak.

In general, there are two ways in which the high strain energy in GaN film is released: one is crack formation and the another is surface roughening.[36–39] Figure 5 shows the GaN surface morphologies measured by the Normaski microscope. There are many cracks found in sample A. With the compressive stress increasing, the number of cracks in the central part of a 2-inch wafer decreases obviously and no crack was found in sample C in the central part of the wafer. It can also be found that the surface of sample C is more flattened with the help of the Normaski microscope. Figure 6 presents the AFM images of GaN films of samples A–C. The root mean square roughnesses (RMS) of the GaN surfaces are 2.78 nm, 0.514 nm, and 0.438 nm respectively and decrease from sample A to sample C. Many pits can be found in sample A and sample B and some protrusions can also be found in sample A. With the compressive stress increasing, no additional pathway such as pits, protrusions or crack formation for strain energy release was needed, as can be seen in Figs. 5 and 6. Relief of strain energy by changing the surface morphology reduces the difference in residual stress between these samples and so the gap is apparently smaller (0.19 GPa). The ω scan FWHMs of the rocking curves of the GaN epitaxial layer of samples A–C are measured by HRXRD and the results are presented in Fig. 7. Both the FWHM values of the (002) and (102) planes get narrower from sample A to sample C, which indicates that the TDD in sample C is the lowest. It can be proven in Figs. 5–7 that a larger compressive stress is beneficial to form a more flattened surface morphology with fewer cracks and have a better crystal quality with a lower TDD in the GaN film.

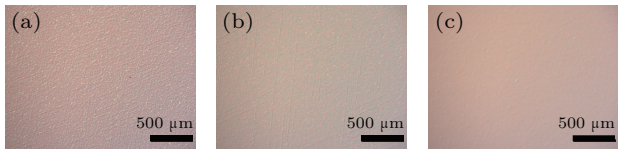


Fig. 5. Normaski microscope images of GaN films deposited on an AlN buffer layer with different lattice parameters: (a) sample A, (b) sample B, (c) sample C.

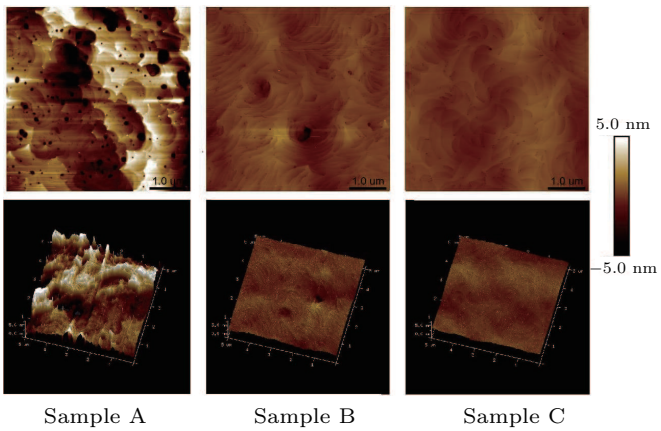


Fig. 6. AFM images (5 μm × 5 μm) of GaN films deposited on an AlN buffer layer with different lattice parameters.

Table 2. Growth conditions of the AlN buffer layer in the orthogonal experiment and the result of lattice parameters measured by HRXRD, where K_1, K_2, and K_3 represent the sum of the lattice parameters for the three levels of each factor and R is the range for each factor. The error in the c-plane lattice parameter is ±0.00006 nm.

	TMA preflow time (s)	Growth rate (nm/s)	Growth temperature (°C)	c-plane lattice parameter (nm)
Exp. 1	20	0.083	1050	0.49707
Exp. 2	20	0.067	1075	0.49693
Exp. 3	20	0.056	1025	0.49655
Exp. 4	30	0.083	1075	0.49690
Exp. 5	30	0.067	1025	0.49748
Exp. 6	30	0.056	1050	0.49643
Exp. 7	60	0.083	1025	0.49689
Exp. 8	60	0.067	1050	0.49727
Exp. 9	60	0.056	1075	0.49691
K_1	1.49055	1.48989	1.49092	
K_2	1.49081	1.49168	1.49077	
K_3	1.49107	1.49086	1.49074	
R	0.00052	0.00179	0.00018	

Finally, we discuss how to better modify the lattice parameter of the AlN buffer layer during growth. A further orthogonal experiment based on samples A to C was done to find which is the key factor that affects the lattice parameter of the AlN buffer layer. The growth conditions and the results of measurement of experiments 1–9 are listed in Table 2, where K represents the sum of the lattice parameter values for the same level of each factor, for example, K_1 for the TMA preflow time is the sum of lattice parameter values in Exp. 1, Exp. 2, and Exp. 3 and the answer is 1.49055. R is the range for each factor which is obtained by subtracting the minimum value from the maximum value of K in the same column. The three variables, i.e., TMA preflow time (20 s, 30 s, 60 s), growth rate of the AlN buffer layer (0.056 nm/s, 0.067 nm/s, 0.083 nm/s) and growth temperature of the AlN buffer layer (1025 °C, 1050 °C, 1075 °C) are set to three different levels in the experiments and the other conditions, such as the thickness of the AlN buffer layer, V/III mole ratio and so on, were kept constant. The calculated range R of different variables can be considered as the degree of correlation between the experimental result and the variables. It was shown that the influence of the growth rate of the AlN buffer layer on lattice parameter values is almost 3.5 times as large as that of TMA preflow time and 10 times as large as that of growth temperature. It is thought-provoking to further explore why the growth rate of the AlN buffer layer, in addition to the preflow condition and growth temperature which were often optimized during the AlN growth,[16,20–23,25] can have such a large influence in effectively affecting the lattice parameter and controlling the stress state. The relation between the lattice parameter and growth rate is presented in Fig. 8. The lattice parameter was acquired by averaging the values in the orthogonal experiment. The largest c-plane lattice parameter (i.e., the smallest in-plane lattice parameter) was obtained at the middle growth rate and the trend is the same as in samples A, B, and C. The exact mechanism of the relation between growth rate and the lattice parameter is still unknown. Here we speculate a possible mechanism as follows. When the growth rate decreases from 0.067 nm/s to 0.053 nm/s, AlN has more time to relax itself from the Si substrate; therefore, the in-plane lattice gets smaller gradually (the in-plane lattice parameter of (111) Si is larger than AlN) and results in a larger c-plane lattice parameter if we assume the process is realized by biaxial stress. As the growth rate increases from 0.067 nm/s to 0.083 nm/s, more TDs are generated in the AlN buffer layer and this process leads to a decrease in interplanar spacing. This is reflected in sample B which had the largest number of TDs as shown in Fig. 3.

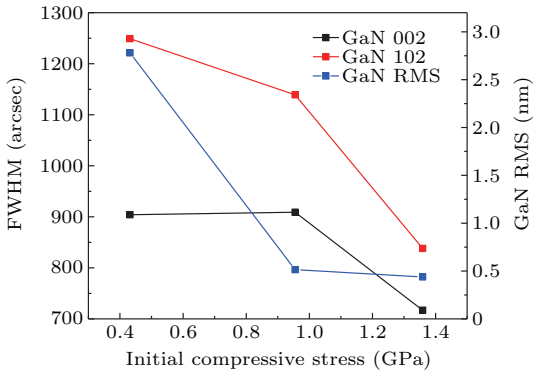


Fig. 7. FWHM of the GaN peak in XRD (002) and (102) rocking curves and the RMS of the GaN surface roughness dependent on initial compressive stress.

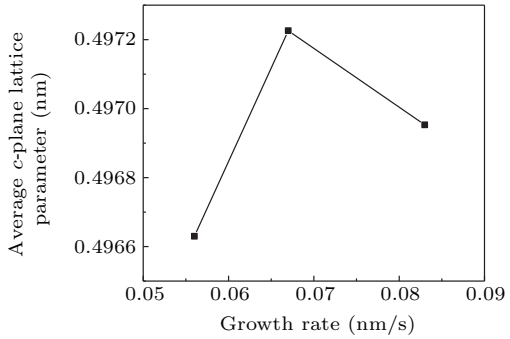


Fig. 8. Average c-plane lattice parameter of the AlN buffer layer in the orthogonal experiment at different growth rates.

4. Conclusion

In summary, in the growth of a GaN/AlN/Si heterostructure system, modulating the lattice parameter of the AlN buffer layer properly by changing the growth rate can help to achieve better stress control and increase the compressive stress at the GaN/AlN heterostructure interface. Meanwhile, a smoother surface morphology of GaN with no pits and lower density of threading dislocations can be obtained with a larger compressive stress. The growth rate of the AlN buffer layer should be an important factor that affects the lattice parameter of the AlN buffer layer as confirmed by an analysis based on a series of orthogonal experiments.

Acknowledgments

Project supported by Beijing Municipal Science & Technology Commission, Administrative Commission of Zhongguancun Science Park (Grant Nos. Z211100007921022 and Z211100004821001), the National Natural Science Foundation of China (Grant Nos. 62034008, 62074142, 62074140, 61974162, 61904172, 61874175, 62127807, and U21B2061), Key Research and Development Program of Jiangsu Province (Grant No. BE2021008-1), Beijing Nova Program (Grant No. 202093), Strategic Priority Research Program of Chinese Academy of Sciences (Grant No. XDB43030101), and Youth Innovation Promotion Association of Chinese Academy of Sciences (Grant No. 2019115).

References

[1] Rathkanthiwar S, Kalra A, Remesh N, Bardhan A, Muralidharan R, Nath D N and Raghavan S 2020 *J. Appl. Phys.* **21** 127
[2] Wang Z, Shan X, Cui X and Tian P 2020 *J. Semicond.* **41** 041606
[3] Zhao D G 2019 *J. Semicond.* **40** 120402
[4] Zhu D, Wallis D J and Humphreys C J 2013 *Rep. Prog. Phys.* **76** 106501
[5] Dadgar A 2015 *Phys. Status Solidi B* **252** 1063
[6] Yu X, Ni J, Li Z, Zhou J and Kong C 2014 *Jpn. J. Appl. Phys.* **53** 051001
[7] Suzuki M, Nakamura A, Nakano Y and Sugiyama M 2017 *J. Cryst. Growth* **464** 148
[8] Pan L, Dong X, Ni J, Li Z, Yang Q, Peng D and Li C 2016 *Phys. Status Solidi C* **13** 181
[9] Cheng J, Yang X, Sang L, Guo L, Zhang J, Wang J, He C, Zhang L, Wang M, Xu F, Tang N, Qin Z, Wang X and Shen B 2016 *Sci. Rep.* **6** 1
[10] Raghavan S, Weng X, Dickey E and Redwing J M 2006 *Appl. Phys. Lett.* **88** 041904
[11] Semond F 2015 *MRS Bull.* **40** 412
[12] Lin K L, Chang E Y, Hsiao Y L, Huang W C, Li T, Tweet D, Maa J S, Hsu S T and Lee C T 2007 *Appl. Phys. Lett.* **91** 222111
[13] Raghavan S, Weng X, Dickey E and Redwing J M 2005 *Appl. Phys. Lett.* **87** 142101
[14] Raghavan S and Redwing J M 2005 *J. Appl. Phys.* **98** 023514
[15] Dai Y, Li S, Sun Q, Peng Q, Gui C, Zhou Y and Liu S 2016 *J. Cryst. Growth* **435** 76
[16] Li Y, Wang W, Li X, Huang L, Zheng Y, Chen X and Li G 2018 *Crystengcomm* **20** 1483
[17] Lee J H and Im K S 2021 *Crystals* **11** 234
[18] Zhen L, Peng P, Qiu C, Zheng B, Armaou A and Zhong R 2020 *Chin. J. Mater. Res.* **34** 744
[19] Lee S J, Jeon S R, Ju J W, Baek J H, Su J, Lee S M, Lee D S and Lee C R 2019 *J. Nanosci. Nanotechnol.* **19** 892
[20] Liu B T, Ma P, Li X L, Wang J X and Li J M 2017 *Chin. Phys. Lett.* **34** 058101
[21] Matsumoto K, Ono T, Honda Y, Murakami S, Kushimoto M and Amano H 2018 *Jpn. J. Appl. Phys.* **57** 091001
[22] Kadir A, Srivastava S, Li Z, Lee K E K, Sasangka W A, Gradecak S, Chua S J and Fitzgerald E A 2018 *Thin Solid Films* **663** 73
[23] Li Y F, Tang C W and Lau K M 2020 *J. Cryst. Growth* **535** 125545
[24] Wei L, Yang X L, Shen J F, Liu D S, Cai Z D, Ma C, He X G, Tang J, Qi S L, Xu F J, Wang X Q, Ge W K and Shen B 2020 *Appl. Phys. Lett.* **116** 232105
[25] Tran B T, Lin K L, Sahoo K C, Chung C C, Lang N C and Chang E Y 2014 *Electron Mater. Lett.* **10** 1063
[26] Dadgar A, Poschenrieder M, Bläsing J, Contreras O, Bertram F, Riemann T, Reiher A, Kunze M, Daumiller I and Krtschil A 2003 *J. Cryst. Growth* **248** 556
[27] Hopcroft M A, Nix W D and Kenny T W 2010 *J. Microelectromech. Syst.* **19** 229
[28] Moram M A and Vickers M E 2009 *Rep. Prog. Phys.* **72** 036502
[29] Thokala R and Chaudhuri J 1995 *Thin Solid Films* **266** 189
[30] Reeber R R and Wang K 2001 *Mrs. Internet J. Nitride Semicond. Res.* **6** 3
[31] Liu J, Huang Y, Sun X, Zhan X, Sun Q, Gao H, Feng M, Zhou Y, Ikeda M and Yang H 2019 *J. Phys. D-Appl. Phys.* **52** 425102
[32] Perlin P, Claude J C, Itie J P, Alfonso S M, Izabella G and Alain P 1992 *Phys. Rev. B* **45** 83
[33] Zhao D M and Zhao D G 2018 *J. Semicond.* **39** 033006
[34] Davydov V Y, Kitaev Y E, Goncharuk I N, Smirnov A N, Graul J, Semchinova O, Uffmann D, Smirnov M B, Mirgorodsky A P and Evarestov R A 1998 *Phys. Rev. B* **58** 12899
[35] Zhao D G, Xu S J, Xie M H, Tong S Y and Yang H 2003 *Appl. Phys. Lett.* **83** 677
[36] Gao H and Nix W D 1999 *Annu. Rev. Mater. Sci.* **29** 173
[37] Gorshkov V N, Tershchuk V V and Sareh P 2021 *Crystengcomm.* **23** 1836
[38] Andersen M and Ghoniem N M 2007 *Fusion Sci. Technol.* **52** 579
[39] Grinfeld M 1993 *J. Nonlinear Sci.* **3** 35